Quantum phase transitions in networks of Lipkin-Meshkov-Glick models

A. V. Sorokin,* V. M. Bastidas,† and T. Brandes
Institut für Theoretische Physik, Technische Universität Berlin, Hardenbergstr. 36, D-10623 Berlin, Germany
(Received 11 July 2014; published 28 October 2014)

We study the quantum critical behavior of networks consisting of Lipkin-Meshkov-Glick models with an anisotropic ferromagnetic coupling. We focus on the low-energy properties of the system within a mean-field approach and the quantum corrections around the mean-field solution. Our results show that the weak-coupling regime corresponds to the paramagnetic phase when the local field dominates the dynamics, but the local anisotropy leads to the existence of an exponentially degenerate ground state. In the strong-coupling regime, the ground state is twofold degenerate and possesses long-range magnetic ordering. Analytical results for a network with the ring topology are obtained.

DOI: 10.1103/PhysRevE.90.042141 PACS number(s): 05.30.Rt, 05.30.Jp, 03.65.Sq

I. INTRODUCTION

The Lipkin-Meshkov-Glick (LMG) model describes an ensemble of all-to-all–coupled two-level systems with anisotropic interactions [1]. This model is complex enough to show quantum phase transitions (QPTs) subject to the change of parameters, but it is exactly solvable in the thermodynamic limit [2]. The total angular momentum that is formed by combining all the spins of single particles is, in this limit, so long that its behavior is close to classical, and the properties of the system can be rather precisely described in the mean-field approximation. From a theoretical point of view, there are proposals to realize the LMG model by means of cavity QED setups [3]. Further theoretical approaches have shown intriguing relations to quantum Fisher information [4] and spin squeezing [5,6]. Experimentally, the dynamics of the LMG model has been explored by using Bose-Einstein condensates [7–10].

Networks of coupled critical systems like LMG models may show new phases with different long- and short-range ordering depending on the topology of the network. In this article, we use Holstein-Primakoff transformations [11] and a mean-field approach to describe quantum phase transitions in a network composed of LMG models with anisotropic ferromagnetic interactions between different sites. Altogether, this restricts us to the lowest energy states only and allows us to study the quantum fluctuations about the mean field. Working in low-energy regions is also the reason for not experiencing any chaotic behavior in the semiclassical limit, even for networks with more than 2 degrees of freedom [12].

Related works used Holstein-Primakoff transformations to describe low-energy magnetic excitations in time-dependent magnetic fields [13] and the interaction of magnons in Heisenberg ferromagnets [14]. Furthermore, in the context of spinor Bose-Einstein condensates [15,16], Holstein-Primakoff transformations can be used to describe the formation of periodic magnetic domains [17].

In most of the articles concerning long-spin chains, the coupling is chosen to have certain continuous symmetries, most commonly by using either isotropic Heisenberg-type or anisotropic coupling [12,17–19]. In this article, however, we focus on the uniaxial coupling, which leads to the existence of a set of global and local discrete symmetries. Thus, the absence of rotational symmetry and the emergence of local discrete symmetries in the problem open the possibility of new effects. Previous works have explored dynamical aspects of networks of coupled systems with global symmetries. For example, the adiabatic phase transitions of networks of qubits have been investigated [20]. In the context of quantum optics, arrays of coupled cavities can exhibit soliton solutions [21], the emergence of phase transitions of light [22], and dissipative quantum phase transitions [23]. Recent theoretical approaches have shown that cold atoms on excited bands in optical lattices could allow for the implementation of networks of nonlinear multiparticle bosonic models exhibiting collective behavior [24,25].

The intriguing properties of spin networks with spatial symmetries have found many experimental implementations. For instance, chains of trapped ions have been shown to undergo a variety of quantum phase transitions when interacting with the laser beams [26]. They have also been used to detect quantum correlations between a two-level system and the environment by measuring the system only [27]. Other experimental implementations of critical spin chains include ultracold polar molecules [28] and Rydberg gases [29] to name but a few.

The structure of this article is as follows. In Sec. II, we describe the model and our bosonization approach. The latter is then used to calculate the ground-state energy analytically in the thermodynamic limit and to identify the different phases of the system. We compare our results with the exact diagonalization of the Hamiltonian in the case of the finite j and the small number of sites N in the chain. In Sec. III, we calculate dispersion relations for the excitation energy in different phases by using Bogoliubov and Fourier transformations. The behavior of the low-energy excitations near phase boundaries is then discussed. In Sec. IV, we calculate correlation functions in the ground state with full translational invariance.

II. THE MODEL

In this article we consider a set of coupled LMG models,

$$\mathcal{H}_l = g J_l^z - \frac{\gamma}{2j}\left(J_l^x\right)^2, \tag{1}$$

*a.sorokin@mailbox.tu-berlin.de
†victor@physik.tu-berlin.de

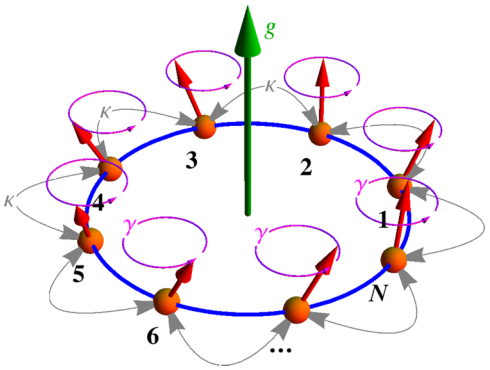

FIG. 1. (Color online) Ring network of LMG models. The coupling between neighboring sites is determined by parameter κ, the strength of interaction within a single site is determined by γ, and g models an external field.

each of which is represented by a node in a network. Throughout the text, g is the strength of an external field and γ determines the self-interaction. We define the ξ component of the collective angular momentum at the lth site $J_l^\xi = \frac{1}{2}\sum_{a=1}^{n}\sigma_{al}^\xi$, where σ_{al}^ξ are Pauli matrices satisfying the algebra $[\sigma_{al}^\xi,\sigma_{bl'}^\nu] = 2i\varepsilon^{\xi\nu\rho}\delta_{ab}\delta_{ll'}\sigma_{al}^\rho$ and the indices $\xi,\nu,\rho \in \{x,y,z\}$ denote the spin components. For a fixed length of the collective angular momentum j, the Hamiltonian (1) undergoes a second-order QPT at $\gamma = g$ [2].

In this article, we study the critical behavior of networks of quantum critical systems by assuming nondirected coupling between the J_y components of the nodes, so the Hamiltonian reads

$$\mathcal{H} = \sum_{l=1}^{N}\mathcal{H}_l - \frac{1}{2j}\sum_{l'\geq l=1}^{N}\kappa_{ll'}J_l^y J_{l'}^y, \tag{2}$$

where $\kappa_{ll'}$ is the coupling matrix of the network [30,31] and $l,l' \in \{1,2,\ldots,N\}$ denote the sites of the chain. The collective angular momentum operators satisfy commutation relations $[J_l^\xi, J_{l'}^\nu] = i\varepsilon^{\xi\nu\rho}\delta_{ll'}J_l^\rho$. In the model, we assume the constants g and γ to be positive, and by choosing $\kappa_{ll'} \geq 0$, we restrict ourselves to ferromagnetic coupling. The model we are considering is a minimal example of critical networks, so we do not look at the antiferromagnetic case $\kappa_{ll'} \leq 0$ here, as that would ask for facing the intricacies of frustration or of the interplay of ferro- and antiferromagnetic couplings [32–34].

Up to Sec. II C, the actual topology of the network is irrelevant, but afterwards it is set to the ring-type one as shown in Fig. 1 by additionally implying periodic boundary conditions $J_{N+1}^\xi \equiv J_1^\xi$. This type of network introduces additional translational symmetry that allows for Fourier transformations and thus simplifies the calculations.

A. Symmetries and limit cases

The Hamiltonian (2) preserves the local angular momentum $[\mathcal{H}, \boldsymbol{J}_l^2] = 0$, where $\boldsymbol{J}_l^2 = (J_l^x)^2 + (J_l^y)^2 + (J_l^z)^2$. Therefore, we can fix j to its maximal value $n/2$ throughout the article. This implies that instead of working in a Hilbert space with the dimension $d = 2^{nN}$, we can restrict ourselves to a subspace with the dimension $d_s = (n+1)^N$ spanned by the basis of tensor products of Dicke states of the individual nodes

$$|j,\boldsymbol{m}\rangle^\xi = \bigotimes_{l=1}^{N}|j,m_l\rangle^\xi, \tag{3}$$

where $\boldsymbol{m} = (m_1,m_2,\ldots,m_N)$, $-j \leqslant m_l \leqslant j$, and ξ denotes the quantization axis. The states $|j,m_l\rangle^\xi$ are eigenstates of the collective angular momentum operators J_l^ξ, such that $J_l^\xi|j,m_l\rangle^\xi = m_l|j,m_l\rangle^\xi$.

The Hamiltonian (2) possesses the global parity

$$\Pi = \exp\left[i\pi\sum_{l=1}^{N}\left(J_l^z + j\right)\right], \tag{4}$$

which is just a product of parities of individual nodes [2,35]. Under the action of Π, the total angular momentum transforms as $\Pi(J_l^x,J_l^y,J_l^z)\Pi^\dagger = (-J_l^x,-J_l^y,J_l^z)$. In the next sections, most importantly in order to perform numerical calculations efficiently, we construct the basis from tensor products of eigenstates of J_l^z. The global parity operator (4) acts on these basis states as $\Pi\,|j,\boldsymbol{m}\rangle^z = (-1)^{\sum_l(m_l+j)}|j,\boldsymbol{m}\rangle^z$, allowing us to separate the Hilbert space into two subspaces—with positive and with negative parity. The positive-parity subspace contains the ground state and has the dimension $d_{s+} = (n+1)^N/2$.

Apart from the global parity (4), the system is also invariant under the local reflection $\mathcal{R}_l^{yz}$ in the yz plane:

$$\begin{aligned}\mathcal{R}_l^{yz} &= \exp\left[i\pi\left(J_l^x + j\right)\right]\exp\left(i\pi J_l^y\right)\mathcal{K}_l \\ &= \exp\left[i\pi\left(J_l^x + j\right)\right]\mathcal{T}_l,\end{aligned} \tag{5}$$

where $\mathcal{T}_l = \exp(i\pi J_l^y)\mathcal{K}_l$ is the time-reversal operator and $\mathcal{K}_l$ is the operator of charge complex conjugation with respect to the standard representation [36] acting on the lth site. The action of the antiunitary local reflection operator on the angular momentum reads $\mathcal{R}_l^{yz}(J_l^x,J_l^y,J_l^z)(\mathcal{R}_l^{yz})^{-1} = (-J_l^x,J_l^y,J_l^z)$.

Now we focus on the analysis of the limit cases to understand the properties of the ground state. For convenience, we introduce the states

$$\left|G^\xi_{p_1,p_2,\ldots,p_N}\right\rangle = \bigotimes_{l=1}^{N}|j,(-1)^{p_l}j\rangle^\xi, \tag{6}$$

where $p_i \in \{0,1\}$ and $\xi \in \{x,y,z\}$.

In the limit $g \gg \gamma,\kappa_{ll'}$, there is a unique ground state $|G\rangle = |G^z_{1,1,\ldots,1}\rangle$—a paramagneticlike state with short-range correlations (cf. Ref. [37]).

In the limit $\gamma \gg g,\kappa_{ll'}$ the ground state is 2^N-fold degenerate and is represented by the set of separable states $|G^x_{p_1,p_2,\ldots,p_N}\rangle$ with all the possible combinations of p_i. In this regime, the system consists of an ensemble of n tightly bound particles with parallel spins along the x direction at each site of the network. The exponential degeneracy of the ground state in this regime is a consequence of the local symmetry (5). It is worth noting that exponentially degenerate ground states arise naturally in the context of spin ice [32] and spin glasses [38].

Finally, in the strong interaction limit $\kappa_{ll'} \gg g,\gamma$, the ground state is highly correlated, twofold degenerate, and includes ferromagnetic states $|G^y_{0,0,\ldots,0}\rangle$ and $|G^y_{1,1,\ldots,1}\rangle$. From the analysis of limit cases we can conclude that the ground states in different limits are drastically different, so the properties between these limits should behave nonanalytically

at some points. This is the onset of the critical behavior that we seek to describe in this article.

B. Bosonization and the ground-state energy

As we are working in the thermodynamic limit, i.e., j is sufficiently large, we can map the angular momentum operators $\boldsymbol{J}_l = (J_l^x, J_l^y, J_l^z)$ onto bosonic operators b_l and $b_l^\dagger$, which satisfy the commutation relations $[b_l, b_{l'}^\dagger] = \delta_{ll'}$ and $[b_l, b_{l'}] = 0$, using Holstein-Primakoff transformations [11]:

$$\begin{aligned} J_l^z &= b_l^\dagger b_l - j, \quad J_l^+ = b_l^\dagger \sqrt{2j - b_l^\dagger b_l}, \\ J_l^- &= \sqrt{2j - b_l^\dagger b_l}\; b_l. \end{aligned} \tag{7}$$

With these transformations, the harmonic approximation around a fixed point is done. In order to obtain the mean-field configurations, we replace the original operators b_l with displaced operators:

$$b_l = \mathcal{D}^\dagger(\alpha_l\sqrt{j})\, d_l\, \mathcal{D}(\alpha_l\sqrt{j}) = d_l + \alpha_l\sqrt{j}, \tag{8}$$

where α_l are the mean fields for each of the nodes, d_l are quantum fluctuations around these, and we define the bosonic displacement operator [39] as

$$\mathcal{D}(\alpha_l\sqrt{j}) = \exp[(\alpha_l d_l^\dagger - \alpha_l^* d_l)\sqrt{j}]. \tag{9}$$

By substituting Eq. (8) into Eq. (7) and expanding the radicals up to $O[(b_l^\dagger b_l/2j)^2]$ as in Refs. [35,40], we get angular momentum operators expressed in terms of α_l and d_l:

$$\begin{aligned} J_l^z &= d_l^\dagger d_l + (\alpha_l^* d_l + \alpha_l d_l^\dagger)\sqrt{j} + (|\alpha_l|^2 - 1)j, \\ J_l^+ &= \sqrt{j(2-|\alpha_l|^2)}(d_l^\dagger + \alpha_l^*\sqrt{j})\left(1 - \frac{c_l}{2} - \frac{c_l^2}{8}\right), \\ J_l^- &= \sqrt{j(2-|\alpha_l|^2)}\left(1 - \frac{c_l}{2} - \frac{c_l^2}{8}\right)(d_l + \alpha_l\sqrt{j}), \end{aligned} \tag{10}$$

with

$$c_l = \frac{d_l^\dagger d_l + (\alpha_l^* d_l + \alpha_l d_l^\dagger)\sqrt{j}}{(2-|\alpha_l|^2)j}.$$

Substituting Eq. (10) into Eq. (2) and truncating higher-order terms we reduce the Hamiltonian to the form

$$\mathcal{H} = E_g(\boldsymbol{\alpha})j + \mathcal{H}_L(\boldsymbol{d},\boldsymbol{\alpha})\sqrt{j} + \mathcal{H}_Q(\boldsymbol{d},\boldsymbol{\alpha}), \tag{11}$$

with $\boldsymbol{\alpha} = (\alpha_1, \alpha_2, \ldots, \alpha_N)$ and $\boldsymbol{d} = (d_1, d_2, \ldots, d_N)$. The terms $\mathcal{H}_L$ and $\mathcal{H}_Q$ are, respectively, linear and quadratic in bosonic operators [41].

The $O(j)$ terms in the expansion of the transformed Hamiltonian add up to form the ground-state energy of the system, which depends on mean fields α_i of each of the nodes and takes the form

$$\begin{aligned} E_g(\boldsymbol{\alpha}) = Ng &- \frac{\gamma}{4}\sum_l (\alpha_l^2 + \alpha_l^{*2}) - \left(\frac{\gamma}{2} + g\right)\sum_l \alpha_l{}^*\alpha_l \\ &+ \frac{\gamma}{8}\sum_l \alpha_l^*\alpha_l(\alpha_l + \alpha_l^*)^2 + \frac{1}{8}\sum_{l'\geq l}\kappa_{ll'} \\ &\times [(\alpha_l - \alpha_l^*)(\alpha_{l'} - \alpha_{l'}^*)\sqrt{2 - \alpha_l^*\alpha_l}\sqrt{2 - \alpha_{l'}^*\alpha_{l'}}]. \end{aligned} \tag{12}$$

We are altogether interested in such $\boldsymbol{\alpha}$ values that would minimize $E_g(\boldsymbol{\alpha})$, as these would correspond to the stable fixed points of the network. The solution of $2N$ simultaneous equations $\{\partial_{\alpha_i} E_g(\boldsymbol{\alpha}) = 0,\ \partial_{\alpha_i^*} E_g(\boldsymbol{\alpha}) = 0\}$, which would give us all the critical points of the surface, cannot be obtained analytically even for N as low as 2. That leaves us with the necessity of locating the critical points numerically.

A related work has shown that under certain conditions the critical points of the energy landscape can be obtained by means of a recurrence relation [12]. In that case, there is an intriguing relation between the recurrence relations defining the fixed points and the stroboscopic dynamics of an effective dynamical system [12]. In our article, however, we are working in a parameter regime where such an approach is not possible.

Another approach we can take—justified both by numerical diagonalization and by symmetry reasons—is to assume that the global minimum (or at least one of the global minima, if they are degenerate) is located at the points of identical mean fields (cf. Ref. [42]). In this case, the ground-state energy becomes a function of only one complex variable $\alpha = \alpha_1 = \cdots = \alpha_N$, and Eq. (12) simplifies to

$$\begin{aligned} E_g(\alpha) = \; & Ng - N\frac{\gamma}{4}(\alpha^2 + \alpha^{*2}) - N\left(\frac{\gamma}{2} + g\right)\alpha^*\alpha \\ & + N\frac{\gamma}{8}\alpha^*\alpha(\alpha + \alpha^*)^2 \\ & + \frac{1}{8}(\alpha - \alpha^*)^2(2 - \alpha^*\alpha)\sum_{l'\geq l}\kappa_{ll'}. \end{aligned} \tag{13}$$

The simultaneous equations $\{\partial_\alpha E_g(\alpha) = 0,\ \partial_{\alpha^*} E_g(\alpha) = 0\}$ can now be solved analytically for an arbitrary network.

Because in the next sections we explore one specific network type, namely, the looped chain (see Fig. 1), we look for the solutions of these equations with $\sum \kappa_{ll'} = N\kappa$. Taking into account the constraint $\alpha^*\alpha \leq 2$ dictated by the reality of the roots in Eq. (12), the only possible critical points in this network are

$$\alpha_g = 0, \quad \alpha_{\gamma\pm} = \pm\sqrt{1 - \frac{g}{\gamma}}, \quad \alpha_{\kappa\pm} = \pm i\sqrt{1 - \frac{g}{\kappa}}. \tag{14}$$

Of these five points, $\alpha_{\gamma\pm}$ exist only in the γ-dominated region (III), $\alpha_{\kappa\pm}$ exist only in the κ-dominated region (II), and α_g is the minimum point only in the g-dominated region (I) (see Fig. 2 for labels of phases).

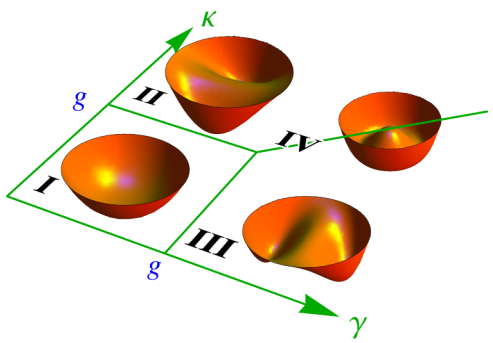

FIG. 2. (Color online) The phase diagram for the ring network of LMG models. The classical energy surfaces $E_g(\alpha)$ are shown in each of the characteristic regions.

The variations of the energy per site $E_g(\alpha)/N$ in the $\gamma\kappa$ space are shown in the left column of Fig. 3 with thick red lines, by assuming the equality of all the mean fields as in Eq. (13). Figure 3 also depicts the exact numerical results for a network with the ring [panels (a) and (b)] and star [panel (c)] topology and a finite number of sites N. As implied by Eq. (13), E_g/N is independent of the number of sites and thus remains the same even in the limit $N \to \infty$. Besides, in regions II and III, E_g depends exclusively on one parameter—κ or γ, respectively—while in region I it is constant.

C. Finite N case

The ansatz we adopted in the previous section, namely, that the mean fields for all the nodes in the network are identical in the ground state, is rather strong and its acceptability needs serious justification. To this end, we performed a direct diagonalization of the Hamiltonian for a network of a finite number of sites N with the topology of a ring by assuming $J^{\xi}_{N+1} \equiv J^{\xi}_1$ and $\kappa_{ll'} = \kappa \neq 0$ iff $l' = l \pm 1$, as well as with the topology of a star by assuming $\kappa_{ll'} = \kappa \neq 0$ iff $l = 1$ or $l' = 1$. Ground-state energy dependence on parameters γ and κ is shown in Fig. 3 for $N = 1$ (single LMG), $N = 3$ (simplest ring), and $N = 4$ (simplest star). The plots for finite angular momentum within each of the nodes ranging from $j = 4$ up to 32 for $N = 1$ or up to 8 for $N = 3$ (thin purple lines) clearly converge to the expected thermodynamic limit acquired using the ansatz from the previous section (thick red lines).

Calculations confirm that the phase diagram of the Hamiltonian (2) is similar to the one of a single anisotropic LMG model with $\gamma_x = \gamma$ and $\gamma_y = \kappa$ [cf. Ref. [2] and Fig. 3(a)], though the physical meaning of the phases is strikingly different. There exist three distinct regions in the phase space (Fig. 2): a "symmetric" g-dominant phase (I) and two "symmetry-broken" κ- and γ-dominant phases (II) and (III), respectively. In phase I, there is only one ground-state energy minimum at $\alpha_1 = \cdots = \alpha_N = \alpha_g$. Due to spontaneous symmetry breaking at the phase boundary, there appear two distinct ground-state energy minima at $\alpha_1 = \cdots = \alpha_N = \alpha_{\kappa\pm}$ in phase II. In phase III, though, E_g is minimized not exclusively for the state with identical mean fields: α_l take either of the two values $\alpha_{\gamma\pm}$ given in Eq. (14), thus making the ground state 2^N-fold degenerate. The degree of degeneracy of the ground state in different phases found numerically coincides with what was expected from the point of view of symmetries in the limit cases in Sec. II A.

At the critical lines ($\gamma = 1, 0 \leq \kappa < 1$), ($0 \leq \gamma < 1, \kappa = 1$), and ($\gamma \geq 1, \kappa = \gamma$) the ground-state energy landscape $E_g(\alpha)$ exhibits a bifurcation, which is a signature of the quantum phase transition [2,35,41]. Besides, as can be concluded from Fig. 3, derivatives of the ground-state energy in the thermodynamic limit with respect to the parameters of the system show no jumps at these lines (see points B and G), allowing us to classify the QPTs occurring here as of the second order. At the line ($\kappa = \gamma > 1$), a QPT also occurs (see point E), but this time the derivative is not continuous and the transition is of the first order.

If we adhere to the identical-mean-field ansatz, then in the thermodynamic limit the coupling term in the Hamiltonian (2) effectively induces a self-interaction in J_y components, reducing $\mathcal{H}$ to the Hamiltonian of a single xy-anisotropic LMG model on the level of the ground-state energy. The difference in the ground-state properties of a network and a single system appears then only in the degeneracy of the ground state in phases II and III.

For further analysis it should be noted that, be the ground state degenerate or nondegenerate, the state with identical mean fields $\alpha_1 = \cdots = \alpha_N = \alpha_{\rm cr}$ with $\alpha_{\rm cr} \in \{\alpha_g, \alpha_{\gamma\pm}, \alpha_{\kappa\pm}\}$ depending on the phase is always a ground state and is used in the following sections as such.

For the calculations of the energy dispersion this does not impose any additional restrictions in phase III, where the ground state is highly degenerate, for the following reasons. Dispersion relations are determined by the quadratic part of the Hamiltonian (11), which can be written as $\mathcal{H}_Q = \boldsymbol{d}^\dagger \mathbb{H} \boldsymbol{d}$, where $(\mathbb{H})_{ll'} = \partial_{\alpha_l \alpha_{l'}} E_g(\boldsymbol{\alpha})$ is the Hessian matrix for $E_g(\boldsymbol{\alpha})$. In phase III, critical points $\alpha_l = \alpha_{\gamma\pm}$ are real, making E_g [see Eq. (12)] an even function in each of the variables α_l due to the local reflection symmetry (5). This means that the second derivatives are even too, making the Hessian and thus $\mathcal{H}_Q$ independent of the choice of the ground state.

III. ENERGY DISPERSION

In this section we focus on the lowest excitation energies of our LMG ring model. As it was justified earlier, the identical-mean-field state with $\alpha_l = \alpha_{\rm cr}$ is a ground state of such a ring and is used throughout this section. The positions of critical points were determined earlier in Eq. (14).

The ansatz about the ground state that was made allows us to calculate energy dispersion relations analytically for an arbitrary large number of sites N in the chain. For this purpose we consider the quadratic part of the Holstein-Primakoff–transformed Hamiltonian (11), which reads

$$\mathcal{H}_Q = L_0 + L_1 \sum_l d_l^\dagger d_l + L_2 \sum_l \left(d_l^2 + d_l^{\dagger 2}\right) + L_3 \sum_l (d_l^\dagger - d_l)(d_{l+1}^\dagger - d_{l+1}), \tag{15}$$

with L_0 through L_3 being factors depending on the parameters of the system and on the critical point in use. For expressions determining these factors see Table I. In order to get rid of nonlocal terms, we map $\mathcal{H}_Q$ onto the reciprocal space using Fourier transformations

$$D_k = \frac{1}{\sqrt{N}} \sum_{l=1}^{N} d_l e^{-ikl} \tag{16}$$

to obtain the $\mathcal{H}_Q$ in terms of Fourier images of d_l:

$$\mathcal{H}_Q = L_0 + L_1 \sum_k D_k^\dagger D_k + L_2 \sum_k (D_k D_{-k} + D_k^\dagger D_{-k}^\dagger) + L_3 \sum_k (D_k D_{-k} e^{-ik} + D_k^\dagger D_{-k}^\dagger e^{ik} - 2 D_k^\dagger D_k \cos k), \tag{17}$$

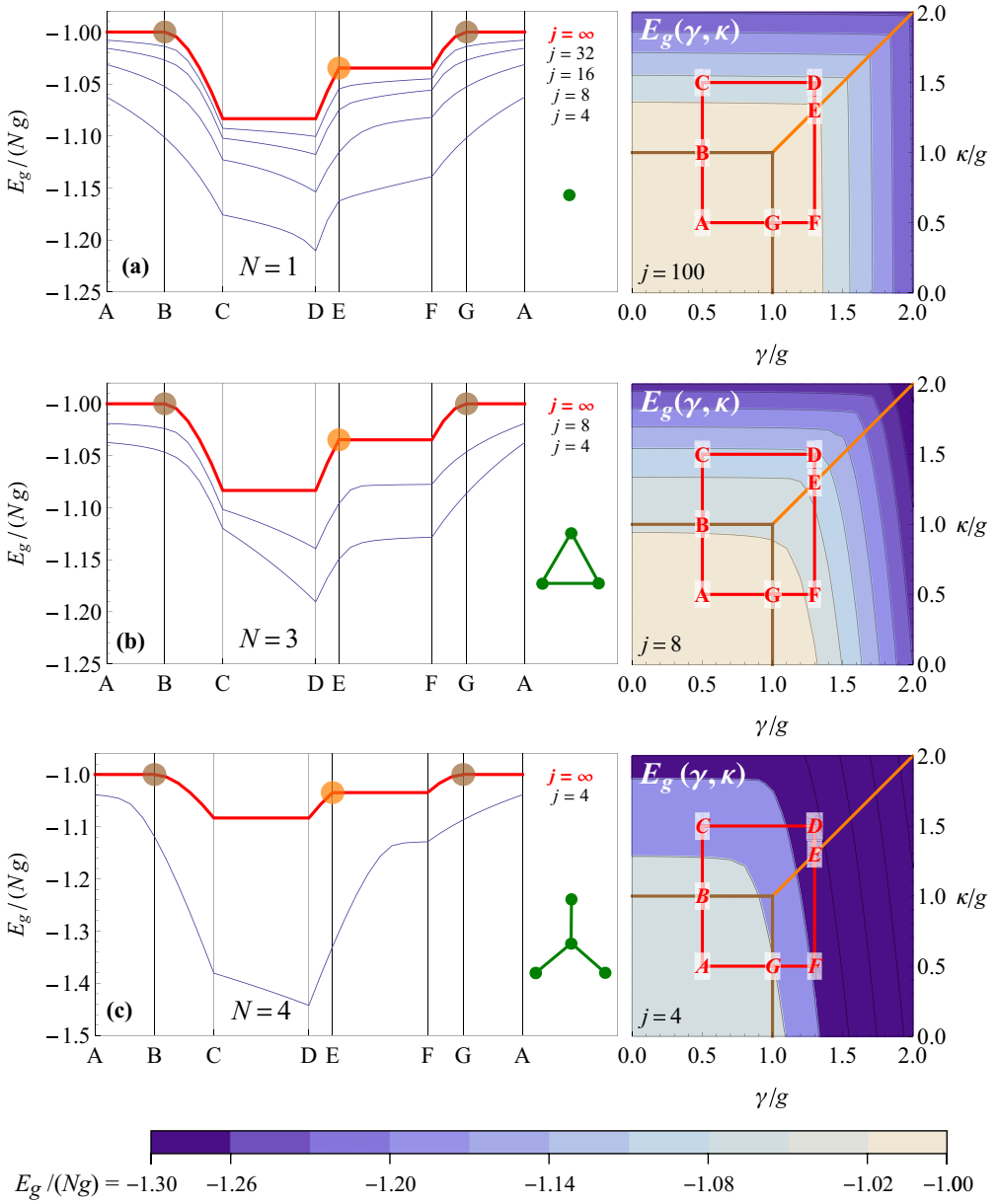

FIG. 3. (Color online) Numerically calculated ground-state energy along the path ABCDEFGA in the $\gamma\kappa$ space (see contour plots) for the LMG rings with the number of sites $N = 1$ (a) and $N = 3$ (b); and the star-type network of $N = 4$ sites (c). Different single-node total angular momentum values are drawn with thin lines; the expected thermodynamic limits are drawn with thick red lines. Contour plots show the ground-state energy for different γ and κ values. Orange (light) lines and circles denote the first-order QPT, while brown (dark) ones denote the second-order QPT.

with $k = 0, 1\frac{2\pi}{N}, \ldots, (N-1)\frac{2\pi}{N}$ and $-k \equiv 2\pi - k$. Fourier transformations preserve commutation relations between bosonic operators, so $[D_k, D_{k'}^\dagger] = \delta_{kk'}$ and $[D_k, D_{k'}] = 0$. In order to simplify this expression, we restrict the sums to

TABLE I. Ground-state energy jE_g and parameters L_0 through L_3 used in Eq. (15) and further on. The ring is initialized in its ground state in the respective region with mean fields $\alpha_l = \alpha_{\rm cr}$.

Region	$\alpha_{\rm cr}$	jE_g	L_0	L_1	L_2	L_3
I	0	$-\mathrm{N\,g\,j}$	$-\frac{1}{2}N\gamma$	$g-\frac{1}{2}\gamma$	$-\frac{1}{4}\gamma$	$\frac{1}{4}\kappa$
II	$\pm i\sqrt{1-g/\kappa}$	$-\frac{1}{2\kappa}Nj(g^2+\kappa^2)$	$-\frac{1}{8}N\left[2\gamma\frac{g+\kappa}{\kappa}-\frac{(\kappa-g)^2}{g+\kappa}\right]$	$\frac{1}{4}\left[4\kappa-2\gamma+\frac{\gamma(\kappa-g)}{\kappa}+\frac{(\kappa-g)^2}{g+\kappa}\right]$	$-\frac{1}{8}\frac{(g^2+2g\kappa)(\gamma-\kappa)+\kappa^2(\gamma+3\kappa)}{\kappa(\kappa+g)}$	$\frac{1}{2}\frac{g^2}{\kappa+g}$
III	$\pm\sqrt{1-g/\gamma}$	$-\frac{1}{2\gamma}Nj(g^2+\gamma^2)$	$\frac{1}{4}N(\gamma-3g)$	$\frac{1}{4}(5\gamma-3g)$	$\frac{1}{8}(3\gamma-5g)$	$\frac{1}{8}\frac{\gamma+g}{\gamma}\kappa$

positive wave numbers, thus getting rid of complex exponents:

$$\mathcal{H}_Q = L_0 + \sum_{k>0} (D_k^\dagger D_k + D_{-k}^\dagger D_{-k})(L_1 - 2L_3 \cos k) + \sum_{k>0} (D_k D_{-k} + D_k^\dagger D_{-k}^\dagger)(2L_2 + 2L_3 \cos k). \quad (18)$$

Then the quadratic part of the Hamiltonian is readily diagonalized by means of Bogoliubov transformations [43]:

$$D_{\pm k} = u_k \beta_{\pm k} - v_k \beta_{\mp k}^\dagger, \quad u_k, v_k \in \mathbb{R}, \qquad u_k^2 - v_k^2 = 1, \quad [\beta_{\pm k}, \beta_{\pm k'}^\dagger] = \delta_{kk'}, \quad (19)$$

which again preserve commutation relations for the new Bogoliubov bosons. After the transformation, $\mathcal{H}_Q$ takes the form

$$\mathcal{H}_Q = L_0 + \sum_k \left[\varepsilon(k) \beta_k^\dagger \beta_k + \frac{1}{2}\varepsilon(k) - \frac{1}{2}\varepsilon_0(k) \right],$$
$$\varepsilon(k) = \sqrt{\varepsilon_0^2(k) - \varepsilon_1^2(k)}, \quad (20)$$
$$\varepsilon_0(k) = L_1 - 2L_3 \cos k, \quad \varepsilon_1(k) = 2L_2 + 2L_3 \cos k,$$

where we return to the summation over all the wave numbers. As the factors L_1 to L_3 do not depend on N, excitation energies $\varepsilon(k)$ are independent of it, too.

We note here for later reference that the products of Bogoliubov coefficients v_k^2 and $u_k v_k$ can be expressed in terms of $\varepsilon(k)$, $\varepsilon_0(k)$, and $\varepsilon_1(k)$ as

$$v_k^2 = \frac{1}{2}\left[\frac{\varepsilon_0(k)}{\varepsilon(k)} - 1 \right] \quad \text{and} \quad u_k v_k = \frac{\varepsilon_1(k)}{2\varepsilon(k)}. \quad (21)$$

Analysis of Eq. (20) shows that the ground-state excitation energy is minimal at $k = 0$ and varies with κ and γ parameters as shown in Fig. 4(d). The energy dispersion is quadratic and gapped in the vicinity of $k = 0$ for parameters away from critical lines. At the phase boundary I-II the gap closes with a linear dispersion [see Fig. 4(a)], denoting, much like in the Ising model, the transition from an unordered paramagnetic phase to the ferromagnetic one. In this case, the softening of the collective excitation leads to long-range correlations resembling the Ising critical point in quantum magnetism [20,22].

At the boundary I-III, on the other hand, the energy gap becomes zero at all the wave numbers [see Fig. 4(b)], thus allowing for the collective excitations of any wavelength and marking the two phases between which the transition occurs as lacking long-range ordering. At the boundary II-III the form of the dispersion relation changes drastically: Approaching the boundary from within phase II, the gap closes with the linear dispersion in the limit $\gamma \to \kappa$, while when approaching the boundary from within phase III, all the modes are gapless in the limit $\kappa \to \gamma$ [Fig. 4(c)]. This jump in the form of the gap closing indicates the first-order QPT.

The linear dispersion around $k = 0$ at the phase boundaries is phononlike and lets us define the group speed $c = (d\varepsilon/dk)_{k=0}$. The way it changes with parameters is shown in Figs. 4(e) and 4(f). At the phase boundary II-III the speed of propagation exhibits a discontinuous behavior, which is another signature of the first-order QPT.

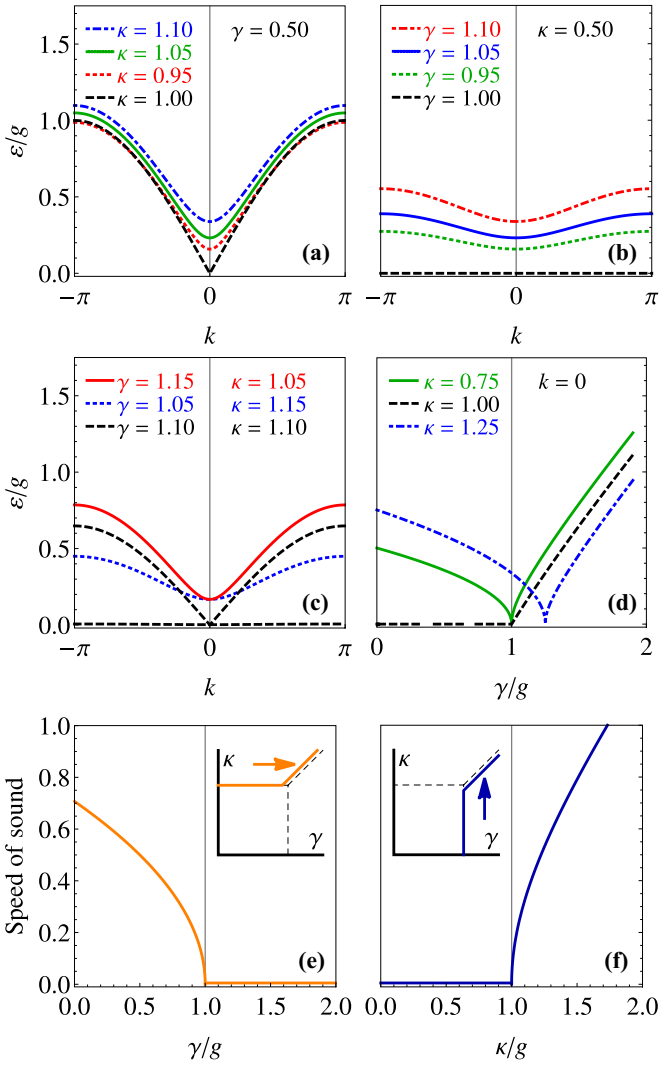

FIG. 4. (Color online) The excitation energy dispersion $\varepsilon(k)$ across the I-II boundary (a), across the I-III boundary (b), and across the II-III boundary (c) as well as the energy gap $\varepsilon(k = 0)$ as a function of γ (d). Panels (e) and (f) show the speed of sound $(d\varepsilon/dk)_{k=0}$ along the phase boundaries.

Now, to obtain the ground state of the Hamiltonian (2) we rely on the diagonalized Hamiltonian (20), from which one can see that the ground state $|G\rangle$ is defined by the condition $\beta_k^\dagger \beta_k |G\rangle = 0$, which leads to the expression

$$|G\rangle = \bigotimes_{k>0} \mathcal{S}(\chi_k)\, \tilde{\mathcal{D}}(\alpha_k \sqrt{j})\, \tilde{\mathcal{D}}(\alpha_{-k}\sqrt{j}) |0_k, 0_{-k}\rangle, \quad (22)$$

where $\alpha_{\pm k} = \frac{1}{\sqrt{N}} \sum_{l=1}^N \alpha_l e^{\mp ikl}$ are the Fourier images of the mean fields and $D_{\pm k}|0_k, 0_{-k}\rangle = 0$. We also have used the displacement operators in the Fourier space [44]

$$\tilde{\mathcal{D}}(\alpha_{\pm k}\sqrt{j}) = \exp[(\alpha_{\pm k} D_{\pm k}^\dagger - \alpha_{\pm k}^* D_{\pm k})\sqrt{j}]. \quad (23)$$

Similarly to Ref. [45], the ground state is a product of two-mode squeezed states with squeezing parameters $\chi_k = \operatorname{artanh}[\varepsilon_1(k)/\varepsilon_0(k)]$, where $\varepsilon_0(k)$ and $\varepsilon_1(k)$ are defined in

Eq. (20). The two-mode squeezing operator [44,45] is

$$\mathcal{S}(\chi_k) = \exp[\chi_k(D_{-k}D_k - D_{-k}^\dagger D_k^\dagger)]. \tag{24}$$

IV. CORRELATION FUNCTIONS

In order to further characterize the phases of the system, it is useful to calculate correlations of some observables between different sites in the ground state for each of the phases. One of the obvious choices is to consider correlations between components of total angular momenta of some site l and a site $l+r$, which is r bonds away from the former. Thus we are interested in functions

$$C_{\xi\xi'}(r) = \frac{1}{2jN}\sum_{l=1}^{N}\langle J_l^\xi J_{l+r}^{\xi'}\rangle_G, \tag{25}$$

where $\xi,\xi' \in \{x,y,z\}$. To simplify the notation we have defined the expectation value of an operator $\mathcal{O}$ in the ground state as $\langle\mathcal{O}\rangle_G = \langle G|\mathcal{O}|G\rangle$. The scaling factor $\frac{1}{2j}$ is introduced to maintain consistency with the original Hamiltonian (2). We now approach the calculation of correlation functions first in limit cases (see Sec. II A) and then take into account the equal-mean-field ansatz.

A. Limit cases

As in Sec. II A, we can look at three limit cases for an arbitrary value of the total angular momentum j. If $g \gg \gamma,\kappa$, the ground state of the system is $|G^z_{1,1,\ldots,1}\rangle$ [see Eq. (6) for notation]. The correlation functions in this state are

$$\begin{aligned}\frac{1}{2j}\langle G^z_{1,1,\ldots,1}|J_l^z J_{l+r}^z|G^z_{1,1,\ldots,1}\rangle &= \frac{j}{2},\\ \langle G^z|J_l^x J_{l+r}^x|G^z\rangle = \langle G^z|J_l^y J_{l+r}^y|G^z\rangle &= 0.\end{aligned} \tag{26}$$

In the limit $\kappa \gg g,\gamma$, the ground state is twofold degenerate, so in order to take both the states into account, we consider a symmetric combination $|G\rangle = \frac{1}{\sqrt{2}}(|G^y_{1,1,\ldots,1}\rangle + G^y_{0,0,\ldots,0}\rangle)$ leading to the following correlation functions:

$$\begin{aligned}\frac{1}{2j}\langle G|J_l^y J_{l+r}^y|G\rangle &= \frac{1}{4j}(j^2+j^2) = \frac{j}{2},\\ \langle G|J_l^x J_{l+r}^x|G\rangle = \langle G|J_l^z J_{l+r}^z|G\rangle &= 0.\end{aligned} \tag{27}$$

In the third limit, $\gamma \gg g,\kappa$, the ground state is 2^N-fold degenerate with different sites having spin projections of either j or $-j$ independently of one another. This limit implies that for a small angular momentum j there is tunneling between different ground states, making all the states have equal probabilities. So, as in the large-κ limit, we consider the ground state to be an equally weighted combination of ground states:

$$|G\rangle = \frac{1}{\sqrt{2^N}}\sum_{p_1,p_2,\ldots,p_N}|G^x_{p_1,p_2,\ldots,p_N}\rangle, \tag{28}$$

with p_i taking values 0 and 1. The z-z and y-y correlations are zero (cf. previous limits), as well as the x-x correlations

$$\langle J_l^x J_{l+r}^x\rangle = \frac{1}{2^{N+1}jN}\sum_l\sum_{p_1,p_2,\ldots,p_N}(-1)^{p_l}(-1)^{p_{l+r}}j^2 = 0. \tag{29}$$

This occurs independent of r, as the pure states $|G^x_{p_1,p_2,\ldots,p_N}\rangle$ are orthogonal and p_l (as well as p_{l+r}) is zero 2^{N-1} times and one another 2^{N-1} times, making the positive terms appear in the sum precisely the same number of times as the negative ones.

It thus may be concluded that in the large-γ limit the system exhibits no correlations whatsoever in any of the components [at least when it is in the state (28)], while large-κ and large-g limits show correlations in the y and z directions, respectively.

B. Equal-mean-field case

In this section we consider correlation functions in a ground state that has full translational invariance. It is important to note that both the paramagnetic and the ferromagnetic ground states inherit this property. In region III, however, due to the exponential degeneracy, there are only two ground states that possess full translational invariance. Other ground states have lower translational symmetry.

Working in the equal-mean-field ansatz we can use the Bogoliubov vacuum (22) as the ground state $|G\rangle$. $C_{\xi\xi'}$ is a sum of correlations of classical background, which are of order j, and correlations of microscopic fluctuations of angular momenta, which are of order 1, much like the Hamiltonian (15) consists of the classical ground-state energy $jE_g \sim O(j)$ and microscopic fluctuations $\mathcal{H}_Q \sim O(1)$ thereupon. (As we consider only minima of E_g, linear terms vanish.)

By calculating both classical and microscopic parts of correlation functions in the limit $r \to \infty$ (implying $N \to \infty$), we can classify the phases according to the long-range ordering. We do it by applying Holstein-Primakoff transformations to the component products followed by Fourier transformations thereof. After these operations we get the following correlations between similar components [restricting wave numbers to positive values of k again, cf. Eq. (18)]:

$$\begin{aligned}C_{\xi\xi}(r) = {}& jM_g + M_0\\ &+ \sum_{k>0}(M_1 \pm 2M_3\cos kr)\langle D_k^\dagger D_k + D_{-k}^\dagger D_{-k}\rangle_G\\ &+ \sum_{k>0}(2M_2 + 2M_3\cos kr)\langle D_k D_{-k} + D_k^\dagger D_{-k}^\dagger\rangle_G,\end{aligned} \tag{30}$$

with parameters M_g and M_0 through M_3 as well as the sign in the first sum defined in Table II. Note that approaching the limit cases where either of the parameters g or κ is much larger than the others, the macroscopic part of correlation functions is in accordance with the functions from the previous section, as in the respective regions the ground state consists of parallel spins. The value of C_{xx} in region III, on the other hand, is different, which is due to the exponential degeneracy of the ground state. If in Sec. IV A, a small total angular momentum j is considered, the tunneling between different states is highly favorable, making the resulting ground state uncorrelated. The equal-mean-field ansatz for large j, though, implies that once initialized in a state with all the spins parallel the system stays in that state and no tunneling occurs resulting in long-range correlations.

TABLE II. Classical correlations jM_g and parameters M_0 through M_3 used in microscopic correlations (31) in regions with ground-state mean fields $\alpha_l = \alpha_{\rm cr}$ between angular momenta components J_i^ξ and J_{i+r}^ξ. The "±" column shows whether in Eq. (31) the upper (+) or the lower (−) sign should be chosen.

Region	$\alpha_{\rm cr}$	ξ	jM_g	M_0	M_1	M_2	M_3	±
		x	0	0	0	0	$\frac{1}{4}$	+
I	0	y	0	0	0	0	$\frac{1}{4}$	−
		z	$\frac{j}{2}$	0	$-\frac{1}{2}$	0	0	+
		x	0	0	0	0	$-\frac{g-\kappa}{8\kappa}$	+
II	$i\sqrt{1-g/\kappa}$	y	$\frac{j}{2}\left(1-\frac{g^2}{\kappa^2}\right)$	$\frac{(g+\kappa)^2}{8\kappa(g-\kappa)}$	$\frac{5\kappa^2+2g\kappa-3g^2}{8\kappa(g-\kappa)}$	$-\frac{3\kappa^2+2g\kappa-g^2}{16\kappa(g-\kappa)}$	$\frac{g^2}{2\kappa(g-\kappa)}$	−
		z	$\frac{j}{2}\frac{g^2}{\kappa^2}$	0	$\frac{g}{2\kappa}$	0	$-\frac{g+\kappa}{2\kappa}$	−
		x	$\frac{j}{2}\left(1-\frac{g^2}{\gamma^2}\right)$	$\frac{(g+\gamma)^2}{8\gamma(g-\gamma)}$	$\frac{5\gamma^2+2g\gamma-3g^2}{8\gamma(g-\gamma)}$	$\frac{3\gamma^2+2g\gamma-g^2}{16\gamma(g-\gamma)}$	$-\frac{g^2}{2\gamma(g-\gamma)}$	+
III	$\sqrt{1-g/\gamma}$	y	0	0	0	0	$\frac{g-\gamma}{8\gamma}$	−
		z	$\frac{j}{2}\frac{g^2}{\gamma^2}$	0	$\frac{g}{2\gamma}$	0	$\frac{g+\gamma}{2\gamma}$	+

Fourier-transformed correlation functions (30) can then be mapped onto Bogoliubov bosons $\beta_k, \beta_k^\dagger$ obtained from diagonalization of the original Hamiltonian taking into account expressions (21) as well as that $\langle\beta_k^\dagger\beta_k\rangle_G = \langle\beta_{-k}^\dagger\beta_{-k}\rangle_G = \langle\beta_k\beta_{-k}\rangle_G = \langle\beta_k^\dagger\beta_{-k}^\dagger\rangle_G = 0$ in the ground state (22).

For a finite size N of the ring, the final expression for the correlation function (30) reads

$$C_{\xi\xi}(r) = jM_g + M_0 + \frac{2}{N}M_1\sum_{k>0}\left[\frac{\varepsilon_0(k)}{\varepsilon(k)} - 1\right] - \frac{4}{N}M_2\sum_{k>0}\frac{\varepsilon_1(k)}{\varepsilon(k)} \pm \frac{2}{N}M_3\sum_{k>0}\cos kr\left[\frac{\varepsilon_0(k)\mp\varepsilon_1(k)}{\varepsilon(k)} - 1\right], \quad (31)$$

where we used Eq. (21) to express Bogoliubov coefficients in terms of $\varepsilon(k)$, $\varepsilon_0(k)$, and $\varepsilon_1(k)$.

In the limit $N\to\infty$, we can rewrite the sums as integrals, assuming $dk \equiv \frac{2\pi}{N}$ to get

$$C_{\xi\xi}(r) = jM_g + M_0 + \frac{M_1}{\pi}\int_0^\pi\left[\frac{\varepsilon_0(k)}{\varepsilon(k)} - 1\right]dk - \frac{2M_2}{\pi}\int_0^\pi\frac{\varepsilon_1(k)}{\varepsilon(k)}dk \pm \frac{M_3}{\pi}\int_0^\pi\left[\frac{\varepsilon_0(k)\mp\varepsilon_1(k)}{\varepsilon(k)} - 1\right]\cos kr\,dk. \quad (32)$$

The macroscopic part of Eq. (32), namely, jM_g, is proportional to the respective projection of any of the angular momenta $[C_{\xi\xi}^{\rm cl} = \frac{1}{2j}(J_l^\xi)^2]$, because we initialize the ring in the ground state where all the angular momenta of different sites are parallel and macroscopically static. Thus $C_{\xi\xi}^{\rm cl}$ is maximized.

The microscopic correlations, too, may be separated into two parts: the background, which is independent of the distance r,

$$C_{\xi\xi}^\infty = \frac{1}{\pi}\int_0^\pi\left\{M_0 + M_1\left[\frac{\varepsilon_0(k)}{\varepsilon(k)} - 1\right] - 2M_2\frac{\varepsilon_1(k)}{\varepsilon(k)}\right\}dk, \quad (33)$$

and oscillations around this background, decaying with r,

$$C_{\xi\xi}^{\rm osc}(r) = \pm\frac{M_3}{\pi}\int_0^\pi\left[\frac{\varepsilon_0(k)\mp\varepsilon_1(k)}{\varepsilon(k)} - 1\right]\cos kr\,dk. \quad (34)$$

In the limit $r\to\infty$ the oscillating part vanishes leaving us with $C_{\xi\xi}(\infty) - jM_g = C_{\xi\xi}^\infty$. Microscopic parts of the correlation functions are plotted in Fig. 5. The plots show that they differ distinctly in different regions only in the background terms $C_{\xi\xi}^\infty$ and the amplitude of the oscillations. The quasiperiod of the oscillations remains the same for all γ and κ.

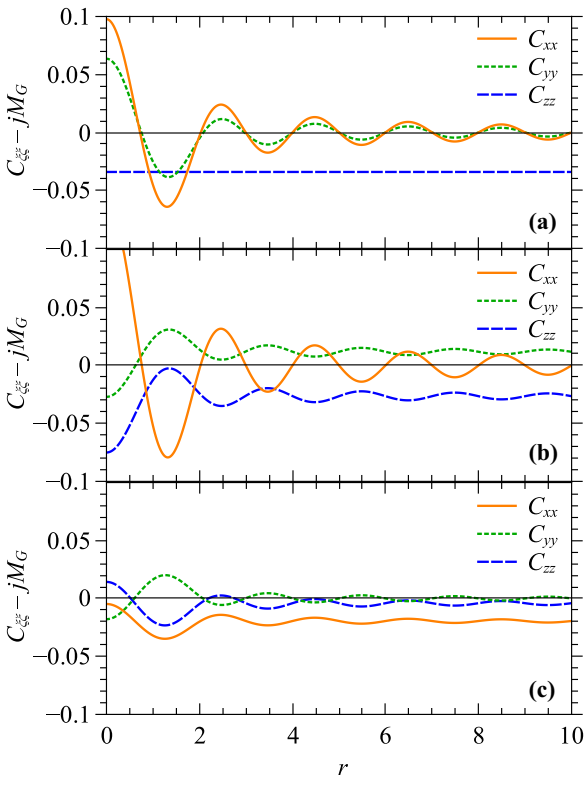

FIG. 5. (Color online) Microscopic parts of correlation functions $C_{\xi\xi}(r) - jM_g$ in region I with $\gamma/g = 0.5$ and $\kappa/g = 0.5$ (a), region II with $\gamma/g = 0.5$ and $\kappa/g = 1.5$ (b), and region III with $\gamma/g = 1.5$ and $\kappa/g = 0.5$ (c).

In region I, only z-z correlations persist in the long-range limit [Fig. 5(a)], repeating the behavior of the macroscopic correlations. The same correspondence between the macroscopic and microscopic correlations is also found in regions II and III. That said, we can classify the phases limiting ourselves to the macroscopic functions without loss of generality to get that the long-range ordering exists in all the phases in corresponding spin components, i.e., in J_z's in region I, J_y's in region II, and J_x's in region III. Note again that the presence of the long-range ordering in region III is subject to tunneling possibility between the ground states and the initial conditions.

Around the phase boundaries, the correlations show particular behavior. For instance, the C_{yy} correlation function flips the sign crossing the boundaries I-II and I-III, and in addition shows an ever growing correlation length approaching I-II. x-x and z-z correlations diverge at I-III. At the phase boundary II-III, C_{xx}, C_{yy}, and C_{zz} show infinite correlation length.

V. CONCLUSIONS

We have discussed the quantum phase transitions in a network of LMG systems coupled via ferromagnetic interactions. In the particular case of a ring topology of the network, we have shown that the ground state can be obtained by calculating the quantum corrections about the mean-field solution. Within the mean-field approach, the ground state can be interpreted as an alignment of angular momenta of the individual sites along the directions that minimize the classical energy of the network. The phase diagram determined from this assumption shows three distinct phases in the $\gamma\kappa$ space in the thermodynamic limit. Such a phase diagram can also be obtained from observing the quantum corrections, i.e., the energy of the collective excitations above the ground state, because the system is gapless along the critical lines [37].

In the particular case of a ground state of the network with full translational invariance, the correlation functions between angular momentum components are clearly distinct for different phases, showing κ- and γ-dominated phases being ferromagnetic in the y and x directions, respectively, and the g-dominated phase showing no long-range ordering. The order parameter increases with the strength of the exchange interaction κ and decreases with the strength of the local interaction γ.

Possible experimental realizations of our model may be based on Bose-Einstein condensates in optical lattices (cf. Refs. [7–10]). Other possibilities include, *inter alia*, single-chain magnets and nanomagnets (cf. Refs. [12,46–48]).

In a recent experiment, by superimposing an optical lattice on a harmonic trap it was possible to create $N = 30$ independent transversely confined BECs. This allows one to perform quantum-enhanced magnetometry by using spin squeezing [49]. In such an experimental setup, our model could be realized by inducing a coupling between the condensates at different sites of the optical lattice. At each site, it is possible to create condensates consisting of up to $n = 600$ atoms. If the dynamics is restricted to two hyperfine levels of the atoms, an on-site linear coupling between the levels could be realized. In addition, the on-site nonlinear terms of the Hamiltonian (2) can be controlled by means of intrawell atom-atom interactions.

In single-chain magnets, the model can be realized by choosing appropriate ligands for magnetic nuclei that would create an easy axis in the chain to induce Ising-like coupling (e.g., as in Ref. [50]). An accurate choice of ligands may also give rise to the quadratic local term in the Hamiltonian [47]. The ring topology used in our work can be realized by cycling the chain as in the related work [18].

As a consequence of finite-size effects, within phase III, there is tunneling between the 2^N ground states, while in phase II, there is tunneling between the two ferromagnetic ground states. The method we have developed in this work can be extended to study other kinds of networks consisting of coupled mean-field-type critical systems, e.g., the Dicke models [35] and spinor Bose gases within the single-mode approximation [15].

Further studies may include the detailed description of the first-order phase transition at the boundary between regions II and III and what happens with correlation functions in its vicinity. In this article we have not considered the issue of antiferromagnetic coupling, i.e., the case when $\kappa_{ll'} \leq 0$. In this context, it would be interesting to explore other topologies of the network to study the emergence of frustration and exotic states such as spin ice [32].

ACKNOWLEDGMENTS

The authors are thankful to Georg Engelhardt, Gernot Schaller, Philipp Strasberg, and Jonas Larson for fruitful discussions and helpful comments and gratefully acknowledge financial support through DFG Grants No. BRA 1528/7, No. BRA 1528/8, No. BRA 1528/9, and No. SFB 910 (V.M.B. and T.B.) and through DAAD Research Grant No. A/12/84446 (A.V.S.).

[1] H. J. Lipkin, N. Meshkov, and A. J. Glick, Nucl. Phys. **62**, 188 (1965); **62**, 199 (1965); **62**, 211 (1965).
[2] P. Ribeiro, J. Vidal, and R. Mosseri, Phys. Rev. Lett. **99**, 050402 (2007).
[3] S. Morrison and A. S. Parkins, Phys. Rev. A **77**, 043810 (2008); Phys. Rev. Lett. **100**, 040403 (2008).
[4] J. Ma and X. Wang, Phys. Rev. A **80**, 012318 (2009).
[5] M. Kitagawa and M. Ueda, Phys. Rev. A **47**, 5138 (1993).
[6] J. Ma, X. Wang, C. P. Sun, and F. Nori, Phys. Rep. **509**, 89 (2011).
[7] C. Gross, T. Zibold, E. Nicklas, J. Estève, and M. K. Oberthaler, Nature (London) **464**, 1165 (2010).
[8] T. Zibold, E. Nicklas, C. Gross, and M. K. Oberthaler, Phys. Rev. Lett. **105**, 204101 (2010).
[9] O. Morsch and M. Oberthaler, Rev. Mod. Phys. **78**, 179 (2006).
[10] G. Theocharis, A. Weller, J. P. Ronzheimer, C. Gross, M. K. Oberthaler, P. G. Kevrekidis, and D. J. Frantzeskakis, Phys. Rev. A **81**, 063604 (2010).
[11] T. Holstein and H. Primakoff, Phys. Rev. **58**, 1098 (1940).

[12] L. Chotorlishvili, Z. Toklikishvili, A. Komnik, and J. Berakdar, Phys. Rev. B **83**, 184405 (2011).
[13] N. Zagury and S. M. Rezende, Phys. Rev. B **4**, 201 (1971).
[14] Z. Cheng, Phys. A **389**, 5671 (2010).
[15] D. M. Stamper-Kurn and M. Ueda, Rev. Mod. Phys. **85**, 1191 (2013).
[16] G. E. Marti, A. MacRae, R. Olf, S. Lourette, F. Fang, and D. M. Stamper-Kurn, Phys. Rev. Lett. **113**, 155302 (2014).
[17] G.-P. Zheng, J.-Q. Liang, and W. M. Liu, Ann. Phys. **321**, 950 (2006).
[18] N. P. Konstantinidis, A. Sundt, J. Nehrkorn, A. Machens, and O. Waldmann, J. Phys.: Conf. Ser. **303**, 012003 (2011).
[19] H. Karimi and I. Affleck, Phys. Rev. B **84**, 174420 (2011).
[20] O. L. Acevedo, L. Quiroga, F. J. Rodríguez, and N. F. Johnson, Phys. Rev. Lett. **112**, 030403 (2014).
[21] I.-H. Chen, Y. Y. Lin, Y.-C. Lai, E. S. Sedov, A. P. Alodjants, S. M. Arakelian, and R.-K. Lee, Phys. Rev. A **86**, 023829 (2012).
[22] M. Schiró, M. Bordyuh, B. Öztop, and H. E. Türeci, Phys. Rev. Lett. **109**, 053601 (2012).
[23] K. Liu, L. Tan, C.-H. Lv, and W.-M. Liu, Phys. Rev. A **83**, 063840 (2011).
[24] F. Pinheiro, J.-P. Martikainen, and J. Larson, Phys. Rev. A **85**, 033638 (2012).
[25] J. Larson, arXiv:1310.7867.
[26] D. Porras and J. I. Cirac, Phys. Rev. Lett. **92**, 207901 (2004).
[27] M. Gessner, M. Ramm, T. Pruttivarasin, A. Buchleitner, H.-P. Breuer, and H. Häffner, Nat. Phys. **10**, 105 (2014).
[28] B. Yan, S. A. Moses, B. Gadway, J. P. Covey, K. R. A. Hazzard, A. M. Rey, D. S. Jin, and J. Ye, Nature (London) **501**, 521 (2013).
[29] P. Schauß, M. Cheneau, M. Endres, T. Fukuhara, S. Hild, A. Omran, T. Pohl, C. Gross, S. Kuhr, and I. Bloch, Nature (London) **491**, 87 (2012).
[30] A. Arenas, A. Díaz-Guilera, J. Kurths, Y. Moreno, and C. Zhou, Phys. Rep. **469**, 93 (2008).
[31] G. Chartrand, *Introductory Graph Theory* (Dover, New York, 1985).
[32] L. Balents, Nature (London) **464**, 199 (2010).
[33] M. Azimi, L. Chotorlishvili, S. K. Mishra, S. Greschner, T. Vekua, and J. Berakdar, Phys. Rev. B **89**, 024424 (2014).
[34] M. Azimi, L. Chotorlishvili, S. K. Mishra, T. Vekua, W. Hübner, and J. Berakdar, New J. Phys. **16**, 063018 (2014).
[35] C. Emary and T. Brandes, Phys. Rev. Lett. **90**, 044101 (2003).
[36] F. Haake, *Quantum Signatures of Chaos*, 3rd ed. (Springer, Berlin, Heidelberg, 2010).
[37] S. Sachdev, *Quantum Phase Transitions*, 2nd ed. (Cambridge University Press, Cambridge, UK, 2011).
[38] K. Binder and A. P. Young, Rev. Mod. Phys. **58**, 801 (1986).
[39] K. E. Cahill and R. J. Glauber, Phys. Rev. **177**, 1857 (1969).
[40] C. Emary and T. Brandes, Phys. Rev. E **67**, 066203 (2003).
[41] M. Hayn, C. Emary, and T. Brandes, Phys. Rev. A **84**, 053856 (2011); **86**, 063822 (2012).
[42] J. Vidal, S. Dusuel, and K. P. Schmidt, Phys. Rev. B **79**, 033109 (2009).
[43] C. J. Pethick and H. Smith, *Bose–Einstein Condensation in Dilute Gases*, 2nd ed. (Cambridge University Press, Cambridge, UK, 2008).
[44] X. Hu and F. Nori, Phys. Rev. Lett. **76**, 2294 (1996).
[45] X.-D. Zhao, X. Zhao, H. Jing, L. Zhou, and W. Zhang, Phys. Rev. A **87**, 053627 (2013).
[46] H.-J. Mikeska and A. K. Kolezhuk, in *Quantum Magnetism*, edited by U. Schollwöck, J. Richter, D. Farnell, and R. Bishop, Lecture Notes in Physics Vol. 645 (Springer, Berlin, Heidelberg, 2004), pp. 1–83.
[47] C. Coulon, H. Miyasaka, and R. Clérac, in *Single-Molecule Magnets and Related Phenomena*, edited by R. Winpenny, Structure and Bonding Vol. 122 (Springer, Berlin, Heidelberg, 2006), pp. 163–206.
[48] W. Wernsdorfer, T. C. Stamatatos, and G. Christou, Phys. Rev. Lett. **101**, 237204 (2008).
[49] W. Muessel, H. Strobel, D. Linnemann, D. B. Hume, and M. K. Oberthaler, Phys. Rev. Lett. **113**, 103004 (2014).
[50] R. Clérac, H. Miyasaka, M. Yamashita, and C. Coulon, J. Am. Chem. Soc. **124**, 12837 (2002).